Characterization and Modeling of CO_2 Transport through Fluorinated Thermoplastics

V. Signorini, L. Ansaloni,* T. Peters, B. Alcock, M. Giacinti Baschetti, and M. Minelli

Read Online

ACCESS | Metrics & More | Article Recommendations | Supporting Information

ABSTRACT: Carbon capture and storage (CCS) is one of the most viable solutions to limit the CO_2 emission in the atmosphere, with the potential to be applied at short-medium time scales. In this concern, polymeric materials play a relevant role in protecting equipment in the CO_2 transport value chain (such as pipelines, pumps, vessels, or compressors). Among the various classes of polymers, fluorinated materials look promising for such application due to their excellent thermal and chemical resistance, combined with a favorable interaction with CO_2 in its supercritical or in a liquid state. This work explores the sorption, diffusion, and permeation properties of various fluorinated thermoplastic polymers when exposed to high-pressure carbon dioxide. Furthermore, the obtained results are analyzed by a thermodynamic equation of state (EoS) to describe the solubility behavior, while the standard transport model (STM) provides a reliable representation of gas transport. That allows the understanding of the penetrant−polymer interaction and the effect of dense phase CO_2 on polymer-based materials in a wide range of temperatures and pressures. The comparison of sorption and transport data by means of the dedicated model allows the reliable prediction of the effects of CO_2 on such fluorinated polymers at all desired temperature and pressure ranges, relevant for CO_2 transport (e.g., dense phase CO_2, up to supercritical conditions).

KEYWORDS: *fluoropolymers, CO_2 sorption, CO_2 diffusion, permeability, carbon capture and storage*
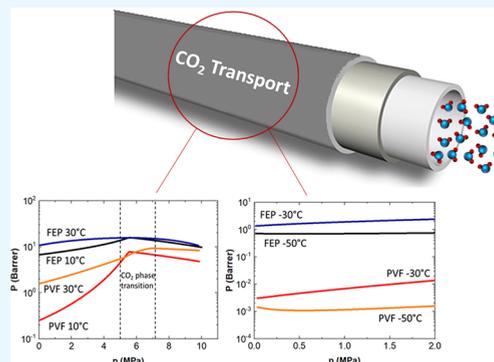
1. INTRODUCTION

Earth's climate has been altered by human beings as a result of the continuous use of fossil fuels and industrial processes.[1] Such massive energy demand has contributed greatly to the accumulation of greenhouse gases in the atmosphere (CO_2, CH_4, and N_2O) that block outward radiation, leading to a rise in the global temperature.[1,2] Significant research effort has been focused on the reduction of CO_2 emissions and limiting climate changes: in this concern, carbon capture and storage (CCS) represents one of the most viable countermeasures that can be implemented in the short-medium term[3] to limit industrial emissions, as well as in the longer period for the decarbonization of hard-to-abate sectors. CCS consists of three main steps: the capture of CO_2 at some stage of industrial processes or energy production plants or by direct capture processes,[4] the subsequent compression of the gas to a dense state and the transportation to the storage site, and finally the injection into suitable CO_2 reservoirs.[5,6]

A well-designed network needs to be created and implemented in order to transfer the captured CO_2 from the emission source to the reservoir site, and to this aim, pipelines and ships are the most promising solutions.[7] This infra-structure, however, needs to be qualified for the transport of CO_2 in a dense state (high pressure and/or low temperature or in a supercritical state), ensuring high efficiency of trans-portation and reduced cost while limiting failures and unwanted emissions.[8]

Pipes, tanks, valves, and many of the other components of the CO_2 transport chain comprise metallic materials due to their mechanical properties, low cost, and well-established use within the industry.[9] However, dense CO_2 streams are characterized by a pronounced corrosivity that may degrade some metallic materials leading to a reduction of their operative lifetime and, consequently, to higher costs or higher risks of failures and or leakages.[10,11] Polymeric materials may also be used in the CO_2 transport value chain, for example, to help to reduce corrosion-related issues, in the sealing elements to prevent leakage, or in the reuse of existing infrastructures where nonmetallic materials are present. In fact, many polymeric liners are already being exploited in the offshore industry for multilayer flexible pipelines (mainly for natural gas transportation) to ensure higher flexibility and resistance to corrosion,[12] while elastomers are used as seals and gaskets.[13]

Despite their current use, little information has been published about the behavior of polymers in the presence of dense carbon dioxide phases: CO_2 transport via pipelines requires operating pressure up to 10−20 MPa at room temperature, above the critical point of CO_2, while ship applications are typically at cryogenic conditions, at pressures in the range of 1−2 MPa and temperature down to −50 °C.[9,14] Moreover, during the transport process, CO_2 can be absorbed significantly in polymers, potentially affecting their mechanical performances or altering the crystallization and glass transition temperatures. CO_2 indeed may be absorbed by some polymers,[15−17] which can cause plasticization phenomena when absorbed in high concentration in the polymeric matrix. This can then lead to issues in case the transport line is subjected to rapid gas decompression (RGD), in which the environmental properties change suddenly, possibly leading to the vaporization of sorbed CO_2 inside the polymer and mechanical damage to the material.[13] Therefore, it is important to investigate the effect that CO_2 has on nonmetallic materials under different temperature and pressure conditions (and physical states) in order to predict the material behavior and their possible failures/damages even under supercritical conditions.

Different polymers behave in distinct manners when in contact with CO_2 according to their intrinsic nature and structure: the morphology (semicrystalline or amorphous), the glass transition temperature (if they are in a glassy or rubbery state), and the molecular structure (free volume) are all relevant parameters that determine both the equilibrium sorption and mass transport behavior. In particular, fully amorphous polymers can exhibit higher CO_2 solubility than to semicrystalline materials due to the lower density and therefore larger free volume of the matrix that better accommodates penetrant molecules.[18−20] The crystalline fraction of semicrystalline polymers also affects the diffusivity of CO_2, which, in general, increases both with penetrant concentration and pressure.[21] The combination of solubility and diffusion coefficient behavior allows the estimation of the permeability in the polymer: the larger the CO_2 diffusion coefficient and solubility, the larger the CO_2 permeability.[22,23]

Although numerous studies reported CO_2 sorption and permeation in polymers, only a few of them are focused on very high pressure, including supercritical conditions,[24,25] mainly due to experimental limitations. However, it has been demonstrated that polymer−penetrant interactions can be reliably described at various temperature, pressure, and compositions using solid thermodynamic and transport models. In fact, CO_2 solubility can be readily predicted by different equation of state (EoS) approaches: the Lattice Fluid Equation of State (LF EoS) by Sanchez and Lacombe,[26] which works well for rubbery or molten polymers, and the Non-Equilibrium Lattice Fluid model (NELF), suitable for glassy materials.[27] On the other hand, the Standard Transport Model (STM) uses the solubility isotherms and the change in the diffusion coefficient with concentration (function of the kinetic mobility coefficient and the thermodynamic factor) to calculate the penetrant permeability at different upstream pressures.[22] In this concern, such modeling scheme has proved to be very reliable in the description of gas permeability behavior as a function of pressure, and it has been demonstrated to be suitable to predict gas solubility and permeability at very high pressure, including supercritical or liquid-like CO_2.[24,28]

Among the various polymeric materials, fluoropolymers (comprising organic polymer chains with some degree of fluorination of the side groups) may be relevant for use in CO_2 transport since they are often used where high temperature or chemical resistance are required. In fact, as reported by de Leon,[29] fluoropolymers are considered as high-performance polymers that can withstand harsh conditions, preserving their intrinsic properties. The C−F bond is the strongest organic bond and gives to the chemical structure an extremely high stability, coupled with a pronounced favorable interaction with CO_2 that leads to appreciable solubilities at high pressures.[17,19,21,30−32] Moreover, this class of materials is relevant for transport of hydrocarbons in the oil and gas infrastructure, due to their outstanding strength and durability, so that they may also be used in CCS transport applications.

In this work, five different examples of semicrystalline fluorinated polymers (polyvinyl fluoride (PVF), poly-(vinylidene fluoride) (PVDF), polytetrafluoroethylene (PTFE), fluorinated ethylene propylene (FEP), and ethylene tetrafluoroethylene (ETFE)) have been investigated. These materials have been experimentally characterized by CO_2 sorption and permeation test at various temperatures in the pressure range between 0 to 3 MPa. Subsequently, a further and rigorous thermodynamic description of the results is applied to CO_2 solubility by an EoS approach, to describe experimental data and to predict the polymer−gas interaction under supercritical conditions. The STM framework is then employed to model the transport of CO_2 in polymers in a wide range of temperatures and pressures by coupling together the solubility and permeability data obtained from the experimental campaign.

2. MATERIALS AND METHODS

2.1. Fluorinated Polymers. The grades of polymeric sheets characterized in this study are reported in Table 1, together with the film thickness. All samples, whose molecular structures are also reported in Table 1, were analyzed as received, with no pretreatment. Sorption and permeation tests were performed by using pure CO_2 (99.99% purity).

Table 1. Properties of Fluoropolymers Analyzed in This Work

Polymer		Thickness [μm]
PVF		50
PVDF		50
PTFE		50
FEP		50
ETFE		100

2.2. Material Characterization. Differential scanning calorimetry (DSC) was performed using a TA Instruments DSC2500, in aluminum pans with an empty pan as reference. Each sample was cooled to −60 °C, heated to an upper temperature T_{max}, cooled to −60 °C, reheated to T_{max}, and cooled to 20 °C at 10 K per minute, with a 5 min isothermal hold at −60 °C at the end of each cooling ramp and a 1 min isothermal hold at T_{max} at the end of each heating ramp. The T_{max} for each polymer was varied to ensure complete melting of each polymer but without heating unnecessarily past the melting point to prevent degradation.[33] T_{max} for each of the polymers was: PVF (230 °C), PTFE (350 °C), PVDF (210 °C), FEP (300 °C), and ETFE (300 °C). Crystallinities for each material were calculated relative to the melting enthalpies of pure crystals of each polymer, as reported in Table 2.

Table 2. Calculated Crystallinity of Polymers Based on the DSC Data in Figure 1

	Melt enthalpy	Heat of Fusion		Crystallinity
Polymer	(from Figure 1)	(J/g)	ref.	(%)
ETFE	40.6	113.4	48	35.8
PVF	64.2	134.3	45	47.8
PVDF	54.8	104.6	46	52.4
PTFE	39.8	82	47	48.5
FEP	16.3	88	48	18.5

2.3. CO₂ Sorption Analysis. Sorption experiments were carried out in the custom-made pressure decay apparatus (the layout is illustrated in Figure S1 of the Supporting Information), which exploits a manometric technique (constant volume and variable pressure) for the determination of gas solubility and diffusivity in a certain amount of polymeric material. The test rig was immersed in a thermostatic bath (Techne TE-10D Tempunit) with a coldfinger (Thermo Haake EK20) as an immersion cooling element for sub ambient temperature tests. A known mass of sample was inserted and sealed into the sample chamber and evacuated under vacuum at least overnight in order to remove any gaseous impurities. The penetrant, CO_2, is loaded into the prechamber compartment at a certain pressure, and the gas sorption is determined by recording the pressure variation between the two compartments (Honeywell pressure transducers PT 01, PT 02 in Figure S1).

Once the gas is filled and the pressure is stable in the prechamber, the connecting valve V03 was opened allowing the gas to diffuse into the material. This volume expansion corresponded to a rapid drop of the pressure, followed by a smoother decrease because the gas is absorbed by the polymer. As soon as the equilibrium pressure is stable to a constant value, valve V03 is closed, and a higher gas pressure is loaded in the prechamber and then expanded again into the sample chamber, proceeding with incremental steps (differential isothermal procedure).

The solubility can be calculated through a mass balance by coupling together eq 1 and eq 2, which account for the amount of gas loaded in the prechamber p_{load}, the gas phase in equilibrium in the sample chamber p_{eq}, and the remaining amount of penetrant at the end of the expansion p_{post}:

$$n_i \text{ [mol]} = n_{i-1} + \frac{p_{load}V_{PC} + p_{post}(V_{SC} - V_{pol}) - p_{eq}(V_{tot} - V_{pol})}{zRT} \tag{1}$$

$$\Omega\left[\frac{g_{CO2}}{g_{pol}}\right] = \frac{n_\infty MW_{CO2}\left[\frac{g}{mol}\right]}{m_{pol}\text{ [g]}} \tag{2}$$

The two equations calculate respectively the moles sorbed at equilibrium (n_i) as a function of the polymer V_{pol} and system volume, V_{tot} (sample chamber V_{sc}, prechamber V_{PC}, and valve volume V_V), and temperature, T, as well as the solubility, Ω, obtained by, first calculating the sorbed mass, from equilibrium sorbed moles, n_∞, and

gas molecular weight, MW_{CO2}, and then dividing it by the initial mass of the polymer m_{pol}. The other parameters present in the equations are the amount of gas already present in the polymer n_0, the universal gas constant R and the compressibility factor z to account for deviation from ideal gas behavior (calculated by using the Peng–Robinson equation of state for CO_2[34]).

The analysis of pressure behavior over time provides sorption kinetics, which allows for the determination of the diffusion coefficient D in the dense polymeric layer, considered as a planar sheet, through the solution to Fick's law provided by Crank:[35]

$$\frac{n_t}{n_\infty - n_0} = 1 - \sum_{i=1}^{\infty} \frac{2\alpha(1+\alpha)}{1+\alpha+\alpha^2 q_i^2} \exp\left(-\frac{4Dq_i^2 t}{l^2}\right) \tag{3}$$

Here n_t is the number of molecules of diffusing substance that entered the layer at time t, l is the thickness of the sheet, q_n are the nonzero positive roots of the equilibrium $\tan q_n = -\alpha q_n$ and $\alpha = 2kV_{tot}/l$, with K being the penetrant partition coefficient between the gas and the polymeric phase.[35]

2.4. CO₂ Permeation. Permeation measurements of carbon dioxide in the different polymer samples were conducted using the constant-pressure method (ASTM D3985-17), employing gas chromatographic (GC) analysis of the permeate stream, in a homemade permeation setup (Figure S2 in Supporting Information). The sample module is placed in a universal oven (Memmert, UF450, Germany) for temperature control. Automated mass flow controllers (MFC, Bronkhorst High-Tech) are used to control the gas supply to the feed and permeate side of the module, respectively. The pressure of the feed side is controlled with an automated back-pressure controller (Bronkhorst High-Tech, P-512C equipped with F-033C control valve, max. 200 bar). At the permeate side, argon is used as sweep gas. The permeate side is always at atmospheric pressure, and the permeate flow is measured using a mass flow meter (MFM, Bronkhorst High-Tech, F-101D, size 100 mL/min). A μ-GC (Agilent 990) equipped with a thermal conductivity detector (TCD) is employed to monitor the gas permeate composition. The gas permeation is calculated from the total permeate flow measured by the MFM and the gas concentration measured by the GC. Permeability values are expressed at 20 °C and 1.013 bar (1 atm) applying unit of Barrer, defined as follows:

$$1\text{ Barrer} = 10^{10}\frac{cm^3(STP)\cdot cm}{cm^2\cdot s\cdot cmHg} = 3.35 \times 10^{-16}\frac{mol\cdot m}{m^2\cdot s\cdot Pa}$$

$$= 7.50 \times 10^{-13}\frac{m^3(STP)\cdot m}{m^2\cdot s\cdot bar} \tag{4}$$

The permeability coefficient for a given gas (P_i) is calculated as

$$\mathcal{P}_i = \frac{\dot{n}_p \cdot y_{i,p} \cdot l}{A \cdot \Delta p_i} \tag{5}$$

where $\dot{n}_p$ is the total molar gas flow on the permeate side calculated from the MFM measurement, $y_{i,p}$ is the ith gas concentration in the permeate side, A is the sample area, l is the sample thickness, and Δp_i is the differential partial pressure of species i between the feed ($p_{f,i}$) and the permeate side ($p_{p,i}$), i.e., the driving force.

3. MODEL DESCRIPTION

Equation of state (EoS) modeling is a solid and rigorous approach for the description of gas–polymer interaction in wide ranges of temperature and pressure, and it can be conveniently used to predict the thermodynamic properties of CO_2/polymer mixtures and the material behavior up to liquid CO_2 or in the supercritical state, relevant to the targeted application.

EoS models can describe amorphous phases only, but they can be applied to the case of semicrystalline polymers assuming that the crystals are impermeable to CO_2, calculating both

solubility and permeability in the amorphous phase only accordingly.[20]

$$\Omega^{am}_{CO_2} = \frac{\Omega^{sc}_{CO_2}}{(1 - \omega_c)} \tag{6}$$

$$p^{am}_{CO_2} = \frac{p^{sc}_{CO_2}}{(1 - \omega_c)^2} \tag{7}$$

where the superscript "*am*" refers to the amorphous phase, while "*sc*" is related to the semicrystalline material (combination of amorphous and crystalline phases).

Such an approach is justified by the larger density of polymer crystallites that are assumed to be impermeable to any kind of penetrant.[20,25] More comprehensive models have been developed to describe gas and vapor solubility[36] or diffusion,[37] based on constraining effects and tortuosity arguments, respectively, but they will not be considered here for the sake of simplicity. The Lattice Fluid model by Sanchez and Lacombe[26] and the nonequilibrium extension of the EoS by the NET-GP model[27] are briefly summarized in the following section.

3.1. LF/NELF Model for CO_2 Solubility.

Equations of state (EoS) provide constitutive laws that correlate pressure, volume, temperature, and internal energy of a substance or a mixture. Such modeling approach is suitable to the description of the solubility isotherm of a generic penetrant into polymers, starting from the intrinsic properties of the pure compounds.[26,38,39] In this concern, the Lattice Fluid (LF) theory by Sanchez and Lacombe[26,40] proved to be reliable and accurate in the representation of the thermodynamic behavior of gas–polymer mixtures in their amorphous/melt state. The whole set of equations are reported in Table S1 in the Supporting Information.

The properties of the pure species (either gas or polymer) are given by three independent parameters: the characteristic temperature T^*, characteristic pressure P^*, and the close-packed density ρ^*:

$$T^* = \frac{\varepsilon^*}{k}, \ P^* = \frac{\varepsilon^*}{v^*}, \ \rho^* = \frac{M}{rv^*} \tag{8}$$

Here ε^* is the interaction energy between two adjacent occupied sites, v^* is the volume of the cell, r is the number of lattice cell occupied by the molecules, and M is the molar mass. These parameters can be retrieved from literature, when present,[27,41] or they can be estimated from pressure–volume–temperature (pVT) measurements of the pure component above their glass transition temperature (T_g) and above their melting temperature (T_m).[42]

For the description of the penetrant/polymer mixture, the characteristic parameters of the pure components are combined by appropriate mixing rules, to determine the binary interaction parameter k_{ij}, which is related to gas–polymer intermolecular interaction.[26,40] This parameter is concentration independent but it can display a weak temperature dependence.

The case of glassy polymers, however, is out of reach for conventional EoS models, due to their intrinsic nonequilibrium nature. Glassy polymers, indeed, are characterized by a lower density than their equilibrium value, and are frozen in an out of the equilibrium condition.[24,26] In this concern, Doghieri and Sarti[27] provided a reliable and comprehensive approach for nonequilibrium thermodynamics as an extension of lattice fluid

EoS (called NELF). The model relies on the assumption that the glass–polymer density may be considered as an internal state variable, which measures the departure from equilibrium.

The description of the volumetric behavior of the polymer phases during sorption is thus an input parameter for the determination of the gas solubility isotherm. Such information can be retrieved from independent dilation data, or even predicted based on rheological arguments.[43] For the sake of simplicity, in this work, a linear behavior of the polymer volume with penetrant pressure has been considered, as often encountered experimentally, and the correlation coefficient K_{Swell} is obtained from the analysis of solubility data:

$$\frac{1}{\rho_{pol}} = \frac{1 + k_{swell}p_i}{\rho^0_{pol}} \tag{9}$$

in which ρ^0_{pol} and K_{Swell} represent the "dry" polymer density the swelling coefficient, respectively.[43,44]

The determination of CO_2 solubility within the frameworks of the Sanchez–Lacombe EoS and the corresponding nonequilibrium extension (NELF) is obtained by the resolution of phase equilibrium in which the chemical potential of the gas equals that in the amorphous polymers, as expressed by eq 10:

$$\mu_i^{pol}(T, p, \Omega, \rho_{pol}) = \mu_i^{gas}(T, p) \tag{10}$$

3.2. Standard Transport Model (STM) for CO_2 Transport.

The STM approach provides a simple and reliable expression for the determination of gas permeability in glassy and rubbery polymer based on temperature, pressure, and concentration. Such a model[22] is based on the definition of diffusive mass flux J_i in polymers (Fick's law).

$$J_i = -\rho D_i \nabla(\omega_i) \tag{11}$$

where ρ is the density of the polymeric material, D is the diffusion coefficient and ω_1 is the mass fraction of i. In a binary (penetrant/polymer) mixture, the diffusion coefficient D can be expressed as the product of the kinetic mobility coefficient L and the thermodynamic factor α, which accounts for the concentration-dependence of the chemical potential μ_i as a driving force.

$$D = L\frac{\partial \mu/RT}{\partial \ln \omega} = L\alpha \tag{12}$$

The combination of the definition of permeability (eq 5) at the steady state, Fick's Law reported in eq 11, and the diffusion coefficient in eq 12, the gas permeability in the amorphous phase can be expressed as follows:[22]

$$p_i = \frac{1}{(p_i^u - p_i^d)} \int_{p_i^d}^{p_i^u} L_\infty e^{\beta\omega_i} S_i z_i \, dp \tag{13}$$

Here p_i^u and p_i^d are the upstream and downstream pressure of the gas at the two sides of membrane layer, respectively; S_i is the solubility coefficient obtained from the phase-equilibrium resolution as a function of pressure (Sanchez–Lacombe or NELF model), while z_i is the penetrant compressibility factor of the pure gas phase (determined by the PR EoS[34]).

L_∞ is the gas infinite dilution mobility coefficient in the polymer (depending on temperature only), while β is the plasticization coefficient that accounts for the increased mobility of the solute with its content in the matrix with an exponential correlation often observed experimentally ($L =$

$L_\infty e^{(\beta \omega)})$.[27] Both terms can be obtained by the best fit of the permeability curves. Finally, it turns out that permeability, as a function of operating pressure, can be calculated from solubility data (via LF/NELF EoS), once the two parameters L_∞ and β are known.[22]

4. EXPERIMENTAL RESULTS

4.1. Material Characterization. The melting endotherms measured by DSC are listed in Figure 1. The crystallinities of these
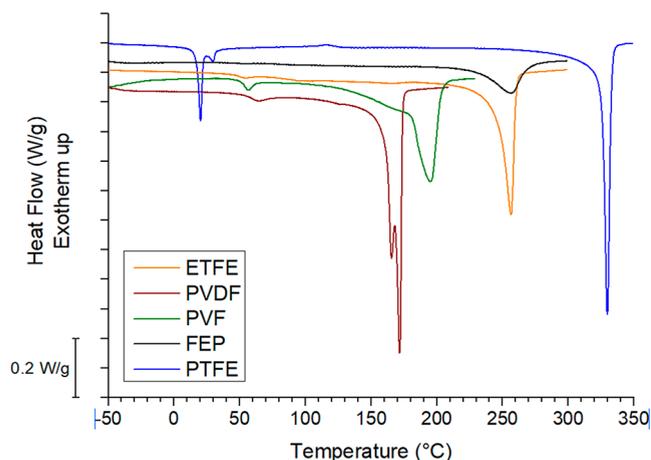

Figure 1. DSC exotherms of polymers investigated in this paper.

samples are calculated based on literature values of the melting enthalpies of 100% crystalline polymers. In addition to the main melting behavior, minor thermal events are also detected, such as endotherms in PTFE at 20 and 30 °C, in PVF and ETFE at 55 °C, and in PVDF at 65 °C. These thermal events are likely to partially alter the morphology of the samples in the temperature regions of

interest for CO_2 transport. However, such effects are expected to play a minor role in the determination of the CO_2 solubility and permeability with respect to the main thermal transitions (melting or glass to rubber), and thus, they are not investigated further in this work. The phase change behaviors of melted, cooled, and remelted samples were similar, but not identical, to the melting behaviors of as received samples, but since the focus of this work is the properties of latter, this is also not discussed further.

4.2. CO_2 Solubility in Fluoropolymers. Pure CO_2 sorption was measured in a temperature range between 6 and 45 °C and in the pressure range 0−3 MPa. The experimental data (symbols) in the semicrystalline polymers are reported as mass ratio as a function of equilibrium pressure in Figure 2 (notice the different y-scale used for sake of clarity), together with the results obtained from the LF/NELF calculations (lines). The absolute error associated with the experimental data is expected to be lower 10%, considering the uncertainty in pressure reading, volumes determination, as well as thermostat accuracy, and the standard deviation in the measurements is within the same values. As expected, the solubility increases by decreasing the operating temperature following the Van't Hoff equation (eq 14):

$$S = S_0 \exp^{(-\Delta H_S / RT)} \tag{14}$$

where S_0 is the pre-exponential factor and ΔH_S is the heat of sorption.[49]

The temperature behavior of the solubility coefficient is reported in Figure S3a in the Supporting Information, together with the obtained values of S_0 and ΔH_S (Table S2). The calculated enthalpy ranges between −17.6 kJ/mol for ETFE and −23.2 kJ/mol for FEP. Even though the five polymers present different glass transition temperatures and different degrees of crystallinity, all isotherms show an almost linear behavior with pressure. Such trend is typical of light gases in low-medium free volume glassy system,[50] as already observed by Bonavoglia et al. for PVDF and PTFE materials.[21,25,51]

It is noteworthy that one of the polymers considered in this work, PVF, has a thermal transition near room temperature attributed to glass transition ($T_g \approx 40$ °C).[52] Therefore, in some of the
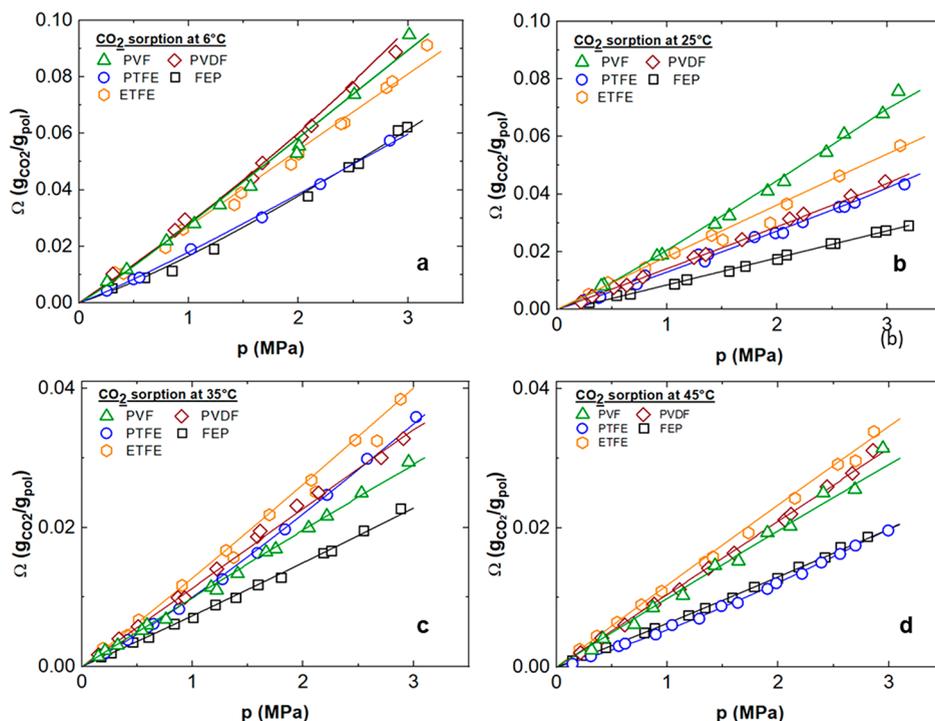

Figure 2. CO_2 solubility in fluoropolymers at 6 °C (a), 25 °C (b), 35 °C (c), and 45 °C (d). Experimental data (empty symbols) are coupled with LF/NELF model curves (lines).
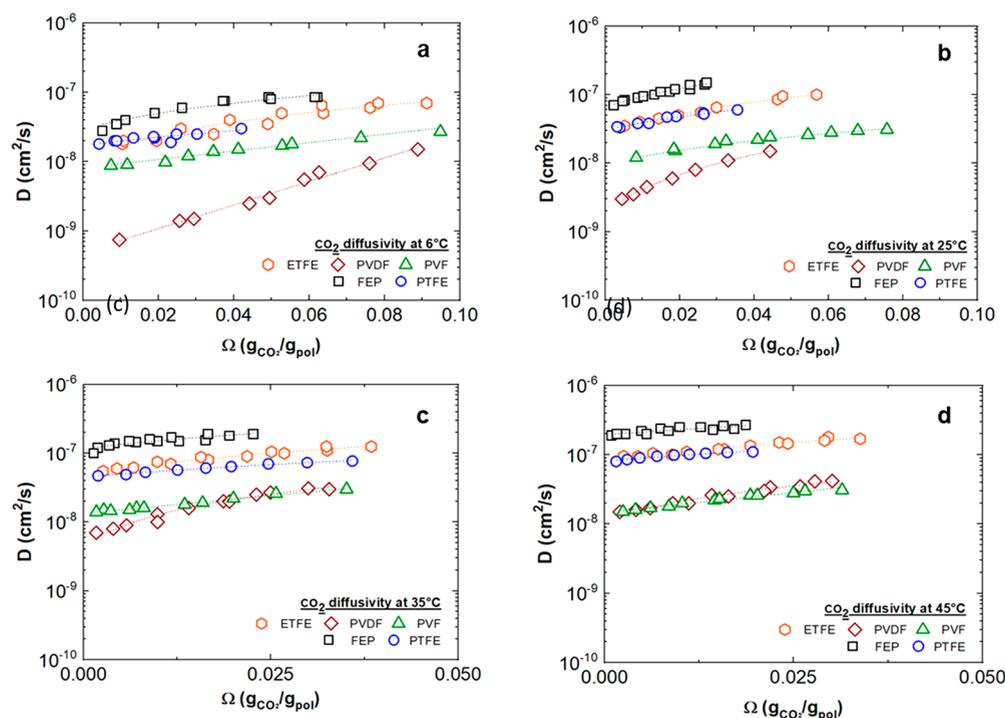
Figure 3. CO_2 diffusivity in fluoropolymers at 6 °C (a), 25 °C (b), 35 °C (c), and 45 °C (d). Lines are guide to the eyes obtained with an exponential correlation for D with respect to solute mass ratio.
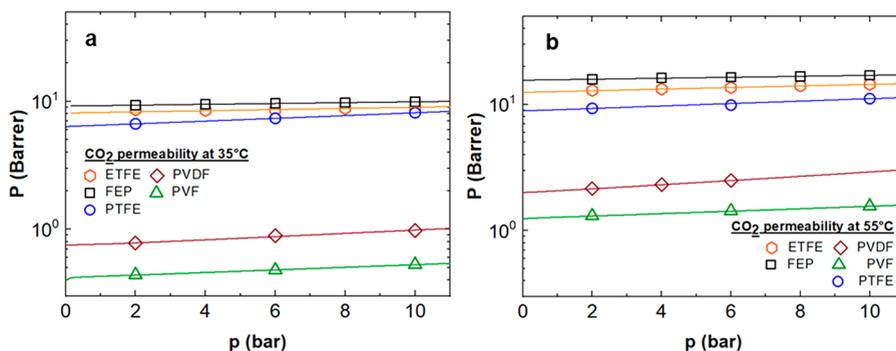

Figure 4. Empty symbols represent experimental isotherms of CO_2 permeability at 35 °C (a) and 55 °C (b) fitted with STM model calculation lines.

experimental conditions explored (6, 25, and 35 °C, see Table 2), the polymer is initially in glassy state, but may become rubbery during the test as CO_2 may act as a plasticizer.[53,54] Unfortunately, that is not clearly visible in the experimental behavior, and no change in sorption concavity can be detected due to the very small excess free volume of glassy PVF,[34] and the near proximity to the glass transition point.

The analysis of sorption kinetics allowed the determination of the CO_2 diffusion coefficient in the different polymers at various temperatures, as indicated in Figure 3, in which the concentration scale (x-axis) has been reduced at 35 and 45 °C to better display the diffusivity behavior. The observed trends pointed out an exponential increase of D with respect to the gas mass fraction (and thus pressure), following the typical behavior often encountered by various penetrants in many polymers, as a consequence of the plasticization effect on the matrix.[31,37] Relevantly, the increase is more significant in some of the fluoropolymers inspected, namely, PDVF, with a diffusion coefficient that is enhanced even more than 1 order of magnitude in the pressure range investigated.

Moreover, the diffusion coefficient is a kinetic parameter that takes into account the energy required by the penetrant to diffuse within the polymeric structure. This behavior might be usually described by

the Arrhenius law within a temperature range investigated, as described by eq 15:

$$D = D_0 \exp^{(-E_D/RT)} \tag{15}$$

Here D_0 is the pre-exponential factor and E_D is the activation energy of diffusion.[37,55]

In the Supporting Information section, Table S2 presents the calculated values for the pre-exponential factor D_0 and the activation energies for diffusion. These values are also plotted in Figure S3b as a function of the inverse of the temperature in order to inspect how the temperature affects diffusion in each material. The activation energy of diffusion ranges from 27.5 (PTFE) to 62.8 kJ/mol (PVDF), proving that diffusion is both a function of temperature, kinetic interaction between the polymer and penetrant, and the polymer morphology.

In the present case, the diffusion coefficient increases by about 1−2 orders of magnitude from 6 to 45 °C, as one can see in Figure 3. PVDF shows the larger sensitivity to temperature, with D enhancements larger than a factor 100 in the range inspected; relevantly, these two materials are also particularly prone to plasticization with a strong D increase as a function of CO_2 concentration.
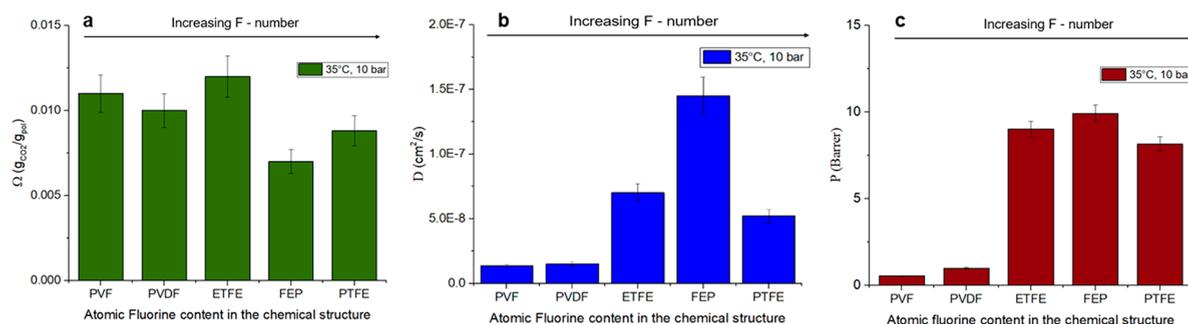
Figure 5. CO_2 solubility (a), CO_2 diffusivity (b), and CO_2 permeability (c) in the semicrystalline polymers as a function of the fluorine content in the monomers structure

4.3. CO_2 Permeability in Fluoropolymers. The CO_2 permeability in all five fluoropolymers is plotted as a function of feed pressure in Figure 4 at the two temperatures (35 and 55 °C) investigated. Even in this case, the absolute error considered within the experimental data elaboration is ca. 10%. As one can see, the permeability increases with both pressure and temperature, similarly to the diffusion coefficient, as commonly observed for incondensable gases in semicrystalline polymers with low free volume. The relationship between solubility, diffusivity, and permeability coefficients obtained is validated by comparing the activation energy of permeation E_a calculated from permeation and transient-sorption experiments. In the first case, E_a has been estimated by applying the Arrhenius law for permeation as a function of temperature, while in the latter one, the activation energy has been determined according to the simplest form of the classical solution-diffusion model, i.e. the sum of ΔH_S and E_D.

The results, reported in Figure S4 in the Supporting Information, prove that the mobility of CO_2 in fluorinated materials can be described as a simple solution-diffusion transport mechanism. The deviation in the two values is indeed limited, and it has to be ascribed to the experimental uncertainties and to the differences related to the different types of measurements.

Relevantly, for the sake of comparison of the CO_2 thermodynamic and transport properties in the different semicrystalline materials, the solubility and diffusion, evaluated at 10 bar (Figures 5a and 5b), and permeability at 10 bar of feed pressure (Figure 5c) have been plotted in order of increasing fluorine content. As one can see, there is no clear correlation of CO_2 uptake and diffusivity with the fluorine content, as the different chemical structures and free volumes of materials affect solubility in a different way. In particular, a large CO_2 solubility in PVF and PVDF corresponds to a small D which results in an extremely low permeability. Such a combination (large S and low P) represents a potential critical issue for the use of these materials in CCS applications due to rapid gas decompression (RGD) issues and plasticization effects.[6,9,56,57] Moreover, the end-side chains present in FEP polymer appear to reduce the amount of gas sorbed by the matrix, while the diffusion coefficient largely increases only for FEP still maintaining an acceptable permeability, thus improving the properties of these materials when exposed to high-pressured CO_2.

In addition, if we consider the crystallinity of the different materials reported in Table 2, as one can see, smaller crystallinity corresponds to a lower solubility in the polymer, as in the case of FEP. Diffusivity and permeability as a consequence are significantly more affected by the amount of crystal present in the structure, as larger ω_c values correspond to low diffusivity and permeability. Such an effect can be readily observed for the case of PVDF.

5. MODELING ANALYSIS

The CO_2 solubility isotherms at different temperatures in the various fluoropolymer determined experimentally are analyzed by the LF/NELF models, and the resulting curves are included in Figure 2. The modeling analysis relied on the characteristic parameters T^*, p^*, and ρ^* of the equilibrium Sanchez–

Lacombe theory for each polymer characterized and for CO_2 gas (Table 3). It is worthwhile to mention that, in this work,

Table 3. LF/NELF Characteristic Parameters of the Penetrant and Fluoropolymers Considered

Polymer	State at RT	p^* [MPa]	T^* [K]	ρ^* [kg/L]	ref
PVF	R/G	610	705	1.39	42
PVDF	R	575	660	1.76	42
PTFE	G	370	605	2.24	42
FEP	G	300	600	2.28	This work
ETFE	G	395	624	1.63	This work
CO_2	Gas	630	300	1.52	27

the parameters for FEP are taken to be equal to those published for PFA due to the absence of literature data, to the best of authors knowledge.[58,59] Such an assumption is motivated from the fact that the two polymers are characterized basically by a similar chemical structure.[60] As reported in other works,[61,62] a deeper analysis on the single contribution of side groups for FEP may provide more accuracy in the prediction of LF polymer–penetrant interaction. However, as already observed by Fossati et al., this approximation for the same type of copolymers does not significantly affect the k_{ij} dependence with temperature in the prediction of gas-solubility coefficient.[63]

Finally, assuming ETFE is a copolymer of ethylene (75 wt %) and tetrafluoroethylene (25 wt %),[64] its characteristic parameters can be estimated using the appropriate mixing rules for the EoS, in a similar fashion to what already done for miscible polymer blends.[23,65]

The lattice fluid model was then employed to describe CO_2 solubility, leading to the determination of the binary interaction parameter k_{ij} for polymers in their rubbery state, and the k_{ij} and k_{swell} coefficients for the glassy materials. Such values were determined and optimized at each temperature by the best fit of CO_2 solubility in the amorphous phase of the polymeric matrix. Both k_{ij} and k_{swell} were found to have a temperature-dependent behavior for all of the polymers investigated. The obtained parameters for all polymers are listed in Table 4.

The STM model described above has been applied to the modeling of CO_2 permeability of the various polymers characterized throughout this work. The parameter values are listed in Table 4, which summarizes all parameters required for the calculation of both the CO_2 permeability and solubility in the range of temperature and pressure inspected. It is evident from Figure 2 that a simple linear dependence of k_{ij} and k_{swell} (for glassy materials only) with temperature represents the

Table 4. LF/NELF and STM Model Parameters for the CO$_2$ Solubility and Diffusivity in the Different Fluoropolymers Inspected

Polymer	CO$_2$ solubility (LF/NELF)		CO$_2$ diffusivity (STM)		
	k_{ij}	k_{swell} (MPa)	L_{∞_am} (cm^2/s) @ 35 °C	β @ 35 °C	E_L (kJ/mol)
PVF	$-4 \times 10^{-4}T + 0.16$	$-1 \times 10^{-3}T + 0.33$	8.6×10^{-9}	23	7.0
PVDF	$-5 \times 10^{-5}T + 0.01$	–	1.3×10^{-8}	26	39.1
PTFE	$-1 \times 10^{-5}T + 0.04$	$-1 \times 10^{-3}T + 0.34$	9.8×10^{-8}	11	46.2
FEP	$1 \times 10^{-3}T + 0.1$	$-1 \times 10^{-4}T + 0.13$	1.2×10^{-7}	19	48.6
ETFE	$-2 \times 10^{-4}T + 0.36$	$-5 \times 10^{-4}T + 0.19$	1.1×10^{-7}	15	34.5
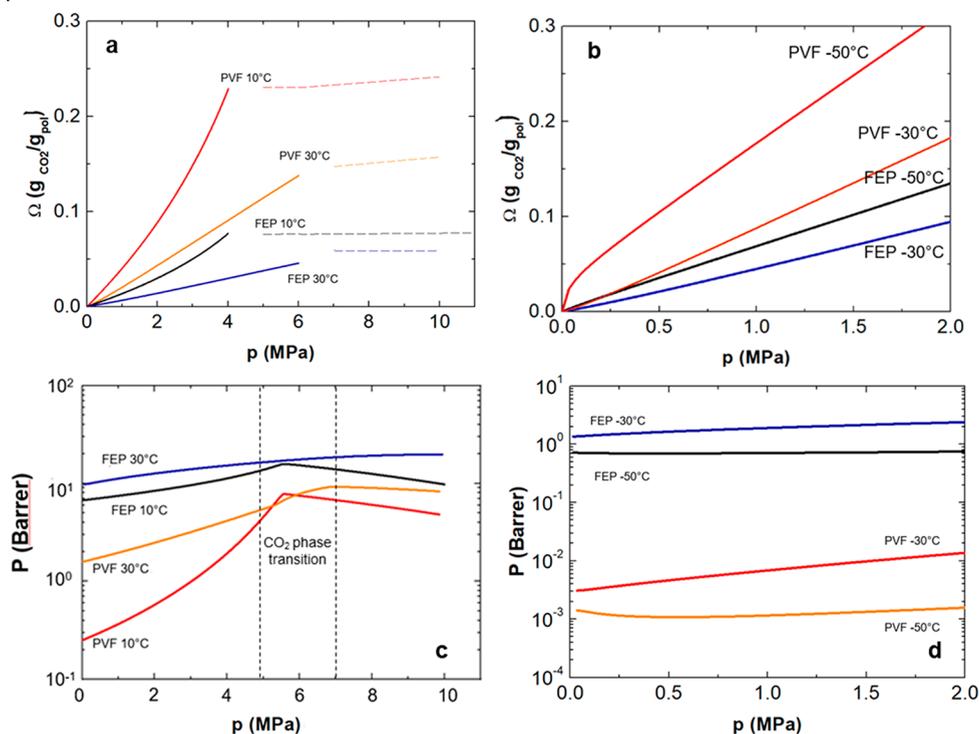
Figure 6. (a) CO$_2$ solubility prediction at 10 and 30 °C (pipeline applications) for PVF and FEP (dashes lines refer to the solubility trend of liquid CO$_2$); (b) CO$_2$ solubility prediction at −30 °C and −50 °C (ship applications) for PVF and FEP; (c) CO$_2$ permeability prediction at 10 and 30 °C (pipeline applications) via STM model for PVF and FEP; (d) CO$_2$ permeability prediction at −30 °C and −50 °C (ship applications) via STM model for PVF and FEP.

experimental trends. The same can be said for the diffusivity modeling, the results of which are shown in Figure 3. The agreement with the experimental trend was remarkable; interestingly, then, the values of the infinite mobility coefficient L_∞ for ETFE and FEP are two times larger than that for PVF at 35 °C.

As one can see, the permeability data at steady state are well described by the STM model, and the determination of the infinite dilute coefficient L_∞ and the plasticization factor is the main modeling output.

The data obtained from the permeability modeling (Table 4) can be compared with the experimental transient sorption characterization, reported in Table S2 in the Supporting Information. The discrepancy between L_∞ and D_0 (note that the thermodynamic factor α is equal to 1 in the limit of infinite dilution) is about 30%, which is in line with experimental uncertainties and modeling errors (Figure S5 in the Supporting Information).

From the values obtained during the experimental characterization at various temperature, we can also predict the solubility and permeability isotherms at operating conditions

useful for carbon transport applications (detailed operating conditions are reported in ref 9) by applying LF/NELF EoS and ST models, respectively. In fact, as briefly mentioned in the introduction, the transport of CO$_2$ occurs via pipelines and/or ships when the gas is compressed to its dense/supercritical state. For this reason, the CO$_2$ sorption and permeability behavior have been predicted at 10 and 30 °C, in a pressure range from 0 to 10 MPa, and at −30 °C and −50 °C (up to 2 MPa), representative operative conditions for CO$_2$ transport via pipelines and ship, respectively.[9,14] The barrier properties of two of the polymers (PVF and FEP) will be examined further since they show very different behaviors in the experimental campaign. In fact, PVF exhibits high solubility, low permeability, and diffusivity, while FEP displays low solubility, high diffusivity, and permeability. The extrapolation for the transport scenario in pipelines and ships is quite large with respect to the experimental characterization performed in this work, in terms of both temperature and pressure. However, both thermodynamic and ST models have already been proved in literature to be extremely reliable in the prediction of CO$_2$ solubility and permeability isotherms either

at covering very wide ranges of temperature (from cryogenic to room values) or pressure (up to supercritical conditions).[24,28]

The results obtained from modeling predictions for the two materials are shown in Figure 6, where the solubility and permeability trends of PVF and FEP are described as a function of temperature and pressure for better understanding the crossing behavior of the polymers close to supercritical CO_2. In particular, in Figures 6a and 6c at 10 and 30 °C (pipelines transport) and in Figures 6b and 6d at −30 and −50 °C (ship transportation), as a function of operating pressure. As one can see, the CO_2 solubility in FEP is predicted to be significantly lower than that in PVF in both scenarios (Figures 6a and 6b). On the other hand, FEP permeability is higher for the two study cases differing about 1 order of magnitude within the two materials (Figures 6c and 6d). Furthermore, CO_2 solubility curves for both PVF and FEP (continuous lines) show an almost linear behavior at low pressure, while, when approaching the vapor−liquid CO_2 transition ($\approx$5−7 MPa), the behavior change significantly (dotted lines). When it reaches the liquid phase, the CO_2 solubility tends to remain constant with pressure due to their inherent property of being incompressible.

As well as the EoS approach, the STM model is able to capture the complex permeability trend of the two materials. Focusing on a pipeline scenario, permeability isotherms show an inflection within 5 and 7 MPa (according to the temperature analyzed), where the transition between vapor-like and liquid-like CO_2 density occurs at the two temperatures investigated, resulting in a decrease of the permeability trend with pressure.[24] This particular behavior at high-CO_2 pressure was already observed by Shamu et al. for the PDMS dense membrane,[66] who attributed it to an increase of the viscosity and density of the fluid which leads to a fall of the diffusion coefficient in the polymer matrix when CO_2 reaches a supercritical regime.

It is worthwhile noting that the use of fluoropolymers as barrier liners in the CCS industry require very specific properties to prevent any material damages that might involve gas leakage.[9,14] In this concern, lower solubility and higher diffusivity are the best threshold combination for CO_2 transport applications, as this combination of parameter is expected to lower the risk of rapid gas decompression damages (less CO_2 is dissolved in the polymer and what is absorbed would be able to escape faster upon sudden changes in the chemical potential of CO_2 in the gas phase).

6. CONCLUSION

Polymers are essential components in the CO_2 transport value chain, required for the deployment of CCS, where they can be used as gaskets, seals, liners, and a protective layer for metal components.

CO_2 solubility, diffusivity, and permeability of examples of five semicrystalline fluorinated polymers that may be relevant for CO_2 transport applications (namely, PVF, PVDF, PTFE, ETFE, and FEP) were investigated in a wide range of temperatures and pressures. The results obtained, both in terms of solubility and permeability of CO_2, in either glassy or rubbery fluoropolymers, were analyzed via appropriate equation of state-based models and the STM approach to predict the penetrant−polymer interaction even in supercritical operating conditions.

CO_2 solubility exhibits a linear pressure-dependence behavior for all the semicrystalline polymers, and it increases

with decreasing the operating temperature. On the CO_2 diffusion coefficient increases with increasing temperature, according to Arrhenius' law, and mass fraction of the gas. In particular, a similar CO_2 sorption behavior is observed for all five materials characterized, while the trends observed for the diffusion coefficient are more affected by the polymer morphology for both temperature and pressure dependence. However, no clear correlation of such behaviors can be observed with the degree of crystallinity neither with the C/F ratio of the atoms in the structures.

Starting from the experimental data obtained for the four temperatures investigated (6, 25, 35, and 45 °C), solubility isotherms of each polymeric material were modeled by means of LF Eos or nonequilibrium NELF model, according to their range of validity. PVDF, since it is rubbery in the temperature range investigated, is modeled by the LF EoS; while the NELF approach was employed for the other glassy polymers, such as PVF, PTFE, ETFE, and FEP.

Moreover, the ST model is applied on experimental CO_2 permeability isotherms with respect to the penetrant pressure, and thanks to the identification of the transport key parameters, it is possible to describe the properties of semicrystalline polymers depending on the concentration of diffusing penetrant. Increasing the crystallinity would likely decrease the absorption of CO_2, reducing the effect of CO_2 on the material properties.

In conclusion, the implementation of LF/NELF and STM equations with experimental sets of data at different temperatures and pressures has proven to be robust and satisfactory for describing the CO_2 uptake and transport over a wide operational range that includes the critical region.

■ ASSOCIATED CONTENT

⑤ Supporting Information

The Supporting Information is available free of charge at https://pubs.acs.org/doi/10.1021/acsapm.3c02056.

> Layouts of CO_2 sorption and CO_2 permeation equipment, table reporting all the parameters used in the modeling investigation, temperature dependence of solubility coefficient according to the van't Hoff equation and diffusion coefficient following the Arrhenius equation, comparison between activation energy of permeability from permeation experiments and from the solution−diffusion mechanism, and the mobility trend calculated from STM modeling (PDF)

■ AUTHOR INFORMATION

Corresponding Author

L. Ansaloni − *SINTEF AS, Oslo 0373, Norway;* ◉ orcid.org/0000-0002-4930-0253; Email: luca.ansaloni@sintef.no

Authors

V. Signorini − *Department of Civil, Chemical, Environmental and Material Engineering (DICAM), Alma Mater Studiorum, University of Bologna, Bologna 40131, Italy*

T. Peters − *SINTEF AS, Oslo 0373, Norway*

B. Alcock − *SINTEF AS, Oslo 0373, Norway*

M. Giacinti Baschetti − *Department of Civil, Chemical, Environmental and Material Engineering (DICAM), Alma Mater Studiorum, University of Bologna, Bologna 40131, Italy*

M. Minelli − *Department of Civil, Chemical, Environmental and Material Engineering (DICAM), Alma Mater Studiorum, University of Bologna, Bologna 40131, Italy;* orcid.org/0000-0003-4662-1526

Complete contact information is available at:
https://pubs.acs.org/10.1021/acsapm.3c02056

Notes

The authors declare no competing financial interest.

■ REFERENCES

(1) Anderson, S.; Newell, R. Prospects for carbon capture and storage technologies. *Annu. Rev. Environ. Resour.* **2004**, *29*, 109−142.

(2) Raza, A.; Gholami, R.; Rezaee, R.; Rasouli, V.; Rabiei, M. Significant aspects of carbon capture and storage - A review. *Petroleum.* **2019**, *5*, 335−340.

(3) Marchetti, C. On geoengineering and the CO2 problem. *Clim. Change.* **1977**, *1*, 59−68.

(4) Bisotti, F.; Ringdal, H.; Rosnes, O.; Mathisen, A.; Hoff, K. A.; Hovland, J. *Direct air capture of CO2 - a review, Norwegian*; VISTA Analyse, SINTEF: 2022..

(5) Boot-Handford, M. E.; Abanades, J. C.; Anthony, E. J.; Blunt, M. J.; Brandani, S.; Mac Dowell, N.; Fernández, J. R.; Ferrari, M. C.; Gross, R.; Hallett, J. P.; Haszeldine, R. S.; Heptonstall, P.; Lyngfelt, A.; Makuch, Z.; Mangano, E.; Porter, R. T. J.; Pourkashanian, M.; Rochelle, G. T.; Shah, N.; Yao, J. G.; Fennell, P. S. Carbon capture and storage update. *Energy Environ. Sci.* **2014**, *7*, 130−189.

(6) Pires, J. C. M.; Martins, F. G.; Alvim-Ferraz, M. C. M.; Simões, M. Recent developments on carbon capture and storage: An overview. *Chem. Eng. Res. Des.* **2011**, *89*, 1446−1460.

(7) Roussanaly, S.; Brunsvold, A. L.; Hognes, E. S. Benchmarking of CO2 transport technologies: Part II - Offshore pipeline and shipping to an offshore site. *Int. J. Greenh. Gas Control.* **2014**, *28*, 283−299.

(8) Johnsen, K.; Helle, K.; Røneid, S.; Holt, H. DNV recommended practice: Design and operation of CO2 pipelines. *Energy Procedia.* **2011**, *4*, 3032−3039.

(9) Ansaloni, L.; Alcock, B.; Peters, T. A. Effects of CO2 on polymeric materials in the CO2 transport chain: A review. *Int. J. Greenh. Gas Control.* **2020**, *94*, 102930.

(10) Zhao, D.; Tian, Q.; Li, Z.; Zhu, Q. A new stepwise and piecewise optimization approach for CO2 pipeline. *Int. J. Greenh. Gas Control.* **2016**, *49*, 192−200.

(11) Cole, I. S.; Corrigan, P.; Sim, S.; Birbilis, N. Corrosion of pipelines used for CO2 transport in CCS: Is it a real problem? *Int. J. Greenh. Gas Control.* **2011**, *5*, 749−756.

(12) Cornacchia, F.; Liu, T.; Bai, Y.; Fantuzzi, N. Tensile strength of the unbonded flexible pipes. *Compos. Struct.* **2019**, *218*, 142−151.

(13) Abas, A. Z.; Nor, A. M.; Suhor, M. F.; Mat, S. Non-metallic materials in supercritical CO2 systems. *Proc. Annu. Offshore Technol. Conf.* **2014**, *3*, 2452−2455.

(14) Tan, Y.; Nookuea, W.; Li, H.; Thorin, E.; Yan, J. Property impacts on Carbon Capture and Storage (CCS) processes: A review. *Energy Convers. Manag.* **2016**, *118*, 204−222.

(15) Goñi, M. L.; Gañán, N. A.; Martini, R. E. Supercritical CO2-assisted dyeing and functionalization of polymeric materials: A review of recent advances (2015−2020). *J. CO2 Util.* **2021**, *54*, 101760.

(16) Tuminello, W. H.; Dee, G. T.; McHugh, M. A. Dissolving Perfluoropolymers in Supercritical Carbon Dioxide. *Macromolecules.* **1995**, *28*, 1506−1510.

(17) Davies, O. R.; Lewis, A. L.; Whitaker, M. J.; Tai, H.; Shakesheff, K. M.; Howdle, S. M. Applications of supercritical CO2 in the fabrication of polymer systems for drug delivery and tissue engineering. *Adv. Drug Delivery Rev.* **2008**, *60*, 373−387.

(18) Doroudiani, S.; Park, C. B.; Kortschot, M. T. Effect of the crystallinity and morphology on the microcellular foam structure of semicrystalline polymers. *Polym. Eng. Sci.* **1996**, *36*, 2645−2662.

(19) Bonavoglia, B.; Storti, G.; Morbidelli, M.; Rajendran, A.; Mazzotti, M. Sorption and Swelling of Semicrystalline Polymers in Supercritical CO2. *J. Polym. Sci., Part B: Polym. Phys.* **2006**, *44*, 1531−1546.

(20) Minelli, M.; De Angelis, M. G. An equation of state (EoS) based model for the fluid solubility in semicrystalline polymers. *Fluid Phase Equilib.* **2014**, *367*, 173−181.

(21) Neela, V.; Von Solms, N. Permeability, diffusivity and solubility of carbon dioxide in fluoropolymers: An experimental and modeling study. *J. Polym. Res.* **2014**, *21*, 401.

(22) Minelli, M.; Sarti, G. C. Permeability and diffusivity of CO2 in glassy polymers with and without plasticization. *J. Membr. Sci.* **2013**, *435*, 176−185.

(23) Minelli, M.; Sarti, G. C. Permeability and solubility of carbon dioxide in different glassy polymer systems with and without plasticization. *J. Membr. Sci.* **2013**, *444*, 429−439.

(24) Ricci, E.; De Angelis, M. G.; Minelli, M. A comprehensive theoretical framework for the sub and supercritical sorption and transport of CO2 in polymers. *Chem. Eng. J.* **2022**, *435*, 135013.

(25) Bonavoglia, B.; Storti, G.; Morbidelli, M. Modeling of the sorption and swelling behavior of semicrystalline polymers in supercritical CO2. *Ind. Eng. Chem. Res.* **2006**, *45*, 1183−1200.

(26) Sanchez, I. C.; Lacombe, R. H. Statistical Thermodynamics of Polymer Solutions. *Macromolecules.* **1978**, *11*, 1145−1156.

(27) Doghieri, F.; Sarti, G. C. Nonequilibrium lattice fluids: A predictive model for the solubility in glassy polymers. *Macromolecules.* **1996**, *29*, 7885−7896.

(28) Minelli, M.; Pimentel, B. R.; Jue, M. L.; Lively, R. P.; Sarti, G. C. Analysis and utilization of cryogenic sorption isotherms for high free volume glassy polymers. *Polymer (Guildf).* **2019**, *170*, 157−167.

(29) de Leon, A. C. C.; da Silva, Í.G.M.; Pangilinan, K. D.; Chen, Q.; Caldona, E. B.; Advincula, R. C. High performance polymers for oil and gas applications. *React. Funct. Polym.* **2021**, *162*, 104878.

(30) Ebnesajjad, S. Chemical Properties of Fluoropolymers—Polytetrafluoroethylene and Polychlorotrifluoroethylene. *Fluoroplastics.* **2015**, *1*, 382−395.

(31) Hedenqvist, M. S.; Ritums, J. E.; Condé-Brana, M.; Bergman, G. Sorption and desorption of tetrachloroethylene in fluoropolymers: Effects of the chemical structure and crystallinity. *J. Appl. Polym. Sci.* **2003**, *87*, 1474−1483.

(32) Lee, S.; Knaebel, K. S. Effects of mechanical and chemical properties on transport in fluoropolymers. I. Transient sorption. *J. Appl. Polym. Sci.* **1997**, *64*, 455−476.

(33) Fontelos, M.; Pizzi, C.; Crafa, G. Non isothermal crystallization of fluoropolymers. *J. Fluor. Chem.* **1992**, *58*, 218.

(34) Peng, D. Y.; Robinson, D. B. A New Two-Constant Equation of State. *Ind. Eng. Chem. Fundam.* **1976**, *15*, 59−64.

(35) Crank, J. *The Mathematics of Diffusion*, 2nd ed.; Claredon Press - Oxford Univ. Press; 1980.

(36) Atiq, O.; Ricci, E.; Baschetti, M. G.; De Angelis, M. G. Modelling solubility in semi-crystalline polymers: a critical comparative review. *Fluid Phase Equilib.* **2022**, *556*, 113412.

(37) Hedenqvist, M.; Gedde, U. W. Diffusion of small-molecule penetrants in semicrystalline polymers. *Prog. Polym. Sci.* **1996**, *21*, 299−333.

(38) Flory, P. J. Statistical Thermodynamics of Liquid Mixtures. *J. Am. Chem. Soc.* **1965**, *87*, 1833−1838.

(39) Flory, P. J. Thermodynamics of polymer solutions. *Discuss. Faraday Soc.* **1970**, *49*, 7.

(40) Lacombe, R. H.; Sanchez, I. C. Statistical thermodynamics of fluid mixtures. *J. Phys. Chem.* **1976**, *80*, 2568−2580.

(41) Rodgers, P. A. Pressure-volume-temperature relationships for polymeric liquids: A review of equations of state and their

characteristic parameters for 56 polymers. *J. Appl. Polym. Sci.* **1993**, *48*, 1061−1080.

(42) Walsh, D.; Zoller, P. *Standard Pressure Volume Temperature Data for Polymers*; 1995; pp 191−215.

(43) Minelli, M.; Doghieri, F. A predictive model for vapor solubility and volume dilation in glassy polymers. *Ind. Eng. Chem. Res.* **2012**, *51*, 16505−16516.

(44) Jordan, S. S.; Koros, W. J. A free volume distribution model for gas sorption and dilation in Glassy polymers. *Macromolecules.* **1995**, *28*, 2228−2235.

(45) Kim, B. S.; Lee, J. Y.; Porter, R. S. The Crystalline Phase Transformation of Poly (Vinylidene Fluoride)/Poly(Vinyl Fluoride) Blend Films. *Polym. Eng. Sci.* **1998**, *38*, 1359−1365.

(46) Benz, M.; Euler, W. B. Determination of the crystalline phases of poly(vinylidene fluoride) under different preparation conditions using differential scanning calorimetry and infrared spectroscopy. *J. Appl. Polym. Sci.* **2003**, *89*, 1093−1100.

(47) Guenoun, G.; Faou, J. Y.; Régnier, G.; Schmitt, N.; Roux, S. PTFE crystallization mechanisms: Insight from calorimetric and dilatometric experiments. *Polymer (Guildf).* **2020**, *193*, 122333.

(48) Walsby, N.; Sundholm, F.; Kallio, T.; Sundholm, G. Radiation-Grafted Ion-Exchange Membranes : Influence of the Initial Matrix on the Synthesis and Structure. *J. Polym. Sci. Part A Polym. Chem.* **2001**, *39*, 3008−3017.

(49) Costello, L. M.; Koros, W. J. Temperature Dependence of Gas Sorption and Transport Properties in Polymers: Measurement and Applications. *Ind. Eng. Chem. Res.* **1992**, *31*, 2708−2714.

(50) Minelli, M.; Sarti, G. C. 110th Anniversary: Gas and Vapor Sorption in Glassy Polymeric Membranes - Critical Review of Different Physical and Mathematical Models. *Ind. Eng. Chem. Res.* **2020**, *59*, 341−365.

(51) Toni, E.; Minelli, M.; Sarti, G. C. A predictive model for the permeability of gas mixtures in glassy polymers. *Fluid Phase Equilib.* **2018**, *455*, 54−62.

(52) Boyer, R. F. Glassy transitions in semicrystalline polymers. *J. Polymer. Sci.: Symposium* **1975**, *50*, 189−242.

(53) Wind, J. D.; Sirard, S. M.; Paul, D. R.; Green, P. F.; Johnston, K. P.; Koros, W. J. Carbon dioxide-induced plasticization of polyimide membranes: Pseudo-equilibrium relationships of diffusion. *sorption, and swelling, Macromolecules* **2003**, *36*, 6433−6441.

(54) Bos, A.; Pünt, I. G. M.; Wessling, M.; Strathmann, H. CO2-induced plasticization phenomena in glassy polymers. *J. Membr. Sci.* **1999**, *155*, 67.

(55) Barrer, R. M.; Skirrow, G. Transport and Equilibrium Phenomena in Gas-Elastomer Systems. II. Equilibrium Phenomena. *Rubber Chem. Technol.* **1949**, *22*, 440−449.

(56) Munkejord, S. T.; Hammer, M.; Løvseth, S. W. CO2 transport: Data and models - A review. *Appl. Energy.* **2016**, *169*, 499−523.

(57) Jeon, S. K.; Kwon, O. H.; Tak, N. H.; Chung, N. K.; Baek, U. B.; Nahm, S. H. Relationships between properties and rapid gas decompression (RGD) resistance of various filled nitrile butadiene rubber vulcanizates under high-pressure hydrogen. *Mater. Today Commun.* **2022**, *30*, 103038.

(58) Dargaville, T. R.; George, G. A.; Hill, D. J. T.; Whittaker, A. K. An investigation of the thermal and tensile properties of PFA following γ-radiolysis. *Macromolecules.* **2003**, *36*, 7132−7137.

(59) Dlubek, G.; Sen Gupta, A.; Pionteck, J.; Häßler, R.; Krause-Rehberg, R.; Kaspar, H.; Lochhaas, K. H. Glass transition and free volume in the mobile (MAF) and rigid (RAF) amorphous fractions of semicrystalline PTFE: A positron lifetime and PVT study. *Polymer (Guildf).* **2005**, *46*, 6075−6089.

(60) G, S. V. *Fluorinated ethylene-propylene copolymers*; Du Pont Nemours E.I. CO., Inc.: 2010; pp 644−656.

(61) Wang, C.; Lei, Z. On the information and methods for calculation of Sanchez-Lacombe and group-contribution lattice-fluid equations of state. *Korean J. Chem. Eng.* **2006**, *23*, 102−107.

(62) High, M. S.; Danner, R. P. Application of the group contribution lattice-fluid EOS to polymer solutions. *AIChE J.* **1990**, *36*, 1625−1632.

(63) Fossati, P.; Sanguineti, A.; De Angelis, M. G.; Baschetti, M. G.; Doghieri, F.; Sarti, G. C. Gas Solubility and Permeability in MFA. *J. Polym. Sci. B: Polym. Phys.* **2007**, *45*, 1637−1652.

(64) Buegman, A. *Permeation-resistance ETFE composition and coatings*; US Patent 6,242,089 B1, 2001.

(65) Grassia, F.; Baschetti, M. G.; Doghieri, F.; Sarti, G. C. *Solubility of Gases and Vapors in Glassy Polymer Blends* **2004**, *876*, 55−73.

(66) Shamu, A.; Dunnewold, M.; Miedema, H.; Borneman, Z.; Nijmeijer, K. Permeation of supercritical CO2 through dense polymeric membranes. *J. Supercrit. Fluids.* **2019**, *144*, 63−70.